Soft Matter

PDMS Polymerized High Internal Phase Emulsions (polyHIPEs) with Closed-cell, Aqueous-filled Microcavities

Journal:	*Soft Matter*
Manuscript ID	SM-ART-08-2019-001732.R1
Article Type:	Paper
Date Submitted by the Author:	18-Oct-2019
Complete List of Authors:	Kataruka, Amrita; University of Illinois at Urbana-Champaign, Civil and Environmental Engg Hutchens, Shelby; University of Illinois at Urbana-Champaign, Mechanical Science and Engineering

Soft Matter

ARTICLE TYPE

Cite this: DOI: 00.0000/xxxxxxxxxx

PDMS Polymerized High Internal Phase Emulsions (polyHIPEs) with Closed-cell, Aqueous-filled Microcavities†

Amrita Kataruka, Shelby B. Hutchens*

Received Date
Accepted Date

DOI: 00.0000/xxxxxxxxxx

Emulsion templates can produce a wide range of unique microstructures via solidification of the continuous phase. Some of these structures result in unique, fluid-filled composites reminiscent of biological tissue when the templating droplets develop into closed-cell structures. However, the state-of-the-art falls short in replicating the mechanical and functional response of biological structures due to stiff, fragile, and bio-incompatible materials while lacking systematic processing parameters. This article describes the synthesis of high internal phase, *closed-cell*, polydimethylsiloxane (PDMS) elastomeric foams which simultaneously achieve biocompatibility, mechanical robustness, flexibility, and selective permeability. Water-in-oil high internal phase emulsions (HIPEs) stabilized by silica nano-particles (SNPs) provide the microstructural template, resulting in a > 74% by volume aqueous phase (up to 82%). To overcome the prohibitive barrier to HIPE formation when using a mechanically-superior, but highly viscous commercial PDMS kit, we produce HIPE templates via centrifugation of low internal phase emulsions (LIPEs, < 30% by volume dispersed phase). This oil phase crosslinks into an aqueous-filled (water + glycerol + NaCl) elastomeric composite. The composite's microstructural dependence on viscosity ratio, mixing speed, emulsifier concentration, and centrifugal force are systematically characterized. The resulting microstructured, fluid-filled elastomer composites exhibit mechanically robust and highly flexible behavior due to the excellent properties of the PDMS continuous phase.

1 Introduction

Traditionally, closed-cell foams utilize gas-forming reactions to produce an unconnected porous structure, prohibiting their ability to encapsulate material within the individual pores. Meanwhile, biology commonly utilizes composite structures characterized by encapsulated, aqueous-filled compartments in the form of tissues to mediate communication, facilitate heterogeneity, and provide structural integrity. Bridging this gap for the production of biomedically-relevant materials requires development of manufacturing strategies that are compatible with ambient conditions (to maintain activity and function in aqueous media) and use non-toxic components. Here we present a strategy that draws upon recent emulsion templating approaches[1,2] to produce highly porous and deformable, aqueous-filled, closed-cell, microstructured monoliths reminiscent of plant tissue (*e.g.*, plant parenchyma). The high internal phase emulsion (HIPE) template used to structure these composites is stabilized using hydrophobic silica nanoparticles.

While many such Pickering emulsion templates produce closed-cell, polymerized HIPEs (polyHIPEs) due to their ability to stabilize droplets against coalescence,[3] the materials previously used are not optimized for biomedical integration. The continuous phase polymer matrix has primarily been limited to solution-polymerizable, often acrylate-based, monomers that typically produce a glassy or semi-crystalline polymer matrix,[4] though a few elastomeric, aqueous-filled composites[5] and hydrogel-filled, semi-crystalline shape memory elastomer composites have been demonstrated.[6] Despite this wide range of HIPE-templated polymeric continuous phases,[2] none can replicate the combination of properties intrinsic to commercial polydimethylsiloxane (PDMS) networks.

Due to its bio-compatibility; chemical, thermal, and mechanical robustness; and cost effectiveness, polydimethylsiloxane (PDMS)-based polymer foams or sponges have shown promise in applications ranging from oil absorption to separation membranes to biomedical support materials.[7] Unfortunately, few microstructural control options for closed-cell, aqueous-filled silicone foams having high volume fraction internal phases are available in the literature. *Closed-cell* PDMS foams are most frequently created

* *University of Illinois at Urbana Champaign, Urbana, United States.*
Tel: +1(217)300-0412; E-mail: hutchs@illinois.edu

† Electronic Supplementary Information (ESI) available: Four pages of supplementary text and figures and two videos. See DOI: 10.1039/cXsm00000x/

via gas-forming reactions,[8–10] prohibiting encapsulation. *Closed-cell* fluid-solid PDMS composites are restricted to medium internal phase emulsions (MIPEs, 30 - 73% volume of dispersed phase)[11] or other low volume fraction composites via more intensive soft patterning techniques,[12,13] and more recently, composites using liquid-metal[14] or polyethylene glycol (PEG)[15] as the high internal phase.

To our knowledge, no *silicone-based*, *closed-cell*, *aqueous-filled* polyHIPEs have been produced, likely due to viscosity-related processing challenges associated with commercially-available polymers or the difficulty of producing high molecular weight silicone in the presence of water. The closest material is reported by Giustiniani *et al.*,[15] HIPE templates formed from reaction stabilized trimethylsiloxy terminated methylhydrosiloxane-co-dimethylsiloxane (MHDS) and water-soluble polyethylene glycol (PEG). These templates utilize milli and micro-fluidic techniques for droplet formation, thereby resulting in highly monodisperse polyHIPEs. Two drawbacks limit this approach: 1) the dispersed phase appears to be limited to PEG as water-in-silicone emulsions led to open-cell foams and 2) at small droplet sizes, micro-fluidic formation is relatively slow. The first drawback limits its potential multifunctional applications of closed-cell, aqueous-filled silicone polyHIPEs made possible by changing the aqueous composite solution. The second limits ultimate sample size and commercialization.

Commercial elastomer kits achieve their mechanical robustness in part due to the strategy of crosslinking long, tailored prepolymers rather than simultaneously polymerizing and crosslinking. These prepolymer solutions are highly viscous, thus using commercially-available PDMS for polyHIPEs requires overcoming key processing challenges associated with its high viscosity relative to an aqueous internal phase. Emulsion template formation depends on fluid phase viscosities, fluid constitutive behaviors, interfacial stabilization methods, and the type of equipment used. For Newtonian fluids, an extensive body of literature describes droplet deformation and breakup under various flow regimes.[16–19] Viscosity ratio, λ, (the dispersed phase viscosity divided by the continuous phase viscosity) plays a key role in determining the ability of a droplet to break apart within the surrounding medium.[17] For a given capillary number, Ca, near a droplet, there exist critical limits at both high and low viscosity ratios for which droplet breakup is suppressed by surface tension. In the case of HIPEs, the viscosity ratio governing droplet breakup relies on the emulsion viscosity (which further increases with increasing dispersed phase); as a result droplet breakup is suppressed at high volume fractions.[20] The prevalence of solution-polymerizable monomers for producing most existing polyHIPE structures becomes clear; two low viscosity fluids require only traditional drop-wise, slow-addition, moderate-speed stirring methods to achieve a dispersed phase volume fraction greater than 74% (*i.e.*, the threshold accepted for a HIPE). The use of a high viscosity continuous phase for a liquid encapsulating polyHIPE has been reported twice to our knowledge: polybutadiene oligomers[21] (the aqueous phase was made more viscous through the addition of sodium alginate) and liquid-metal-in-PDMS (two high viscosity fluids).[14] However, restrictions on droplet breakup for an ultra low viscosity ratio between liquid phases, such as that created using high molecular weight PDMS and water, critically limits the volume of dispersed phase, severely restricting emulsion formation.

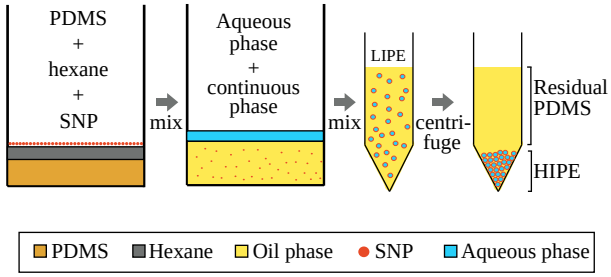

Fig. 1 Schematic illustration of the high internal phase emulsion (HIPE) fabrication procedure.

In this manuscript, we provide a detailed account of how to overcome these challenges to fabricate closed-cell, aqueous-filled PDMS polyHIPEs from inexpensive, commercially-available silicone. We quantify the limitations associated with their formation as well as the processing parameters that may be tuned to adjust the cellular structure. We first overview the emulsion template and polyHIPE fabrication and characterization methods used. Mechanisms for emulsion formation limits and droplet control are discussed and quantified. We employ centrifuged low internal phase emulsions (LIPEs) as templates for the polyHIPEs. The dependence of polyHIPE structure, especially the stability of the closed-cell cavities, on centrifugation force and emulsifier are reported. We provide an example of how the process may be modified to produce open-cell polyHIPEs.

2 Methods

2.1 Emulsion Preparation

Unless otherwise stated, the oil phase consists of an uncured polydimethylsiloxane (PDMS) kit (Solaris, *Smooth-On*), and hexane (H-3341, *Fischer Scientific*). Silica nanoparticles (SNPs) (Aerosil R974, *Evonik Corporation*) stabilze the emulsion. Oil phase and stabilizer are mixed (30 s; 3500 rpm; dual asymmetric centrifugal (DAC) mixer, *FlackTek Inc.*) to form the continuous phase before being combined with the aqueous phase. The aqueous phase consists of 0.1 M NaCl in a 2:1 ratio water:glycerol (by weight) mix. Unless otherwise stated, the aqueous phase is incorporated into the continuous phase in two steps—gentle, manual mixing followed by DAC mixing (30 s). Composition and processing parameters were varied over the parameter ranges in Table 1.

2.2 Viscosity Measurement

Viscosity measurements use a 40 mm diameter, temperature controlled, aluminum parallel-plate geometry at 1 mm gap across a frequency range of 10-300 Hz (AR-G2 rheometer, TA instruments). A solvent trap minimizes hexane evaporation. Viscosity plateaus after a shear rate of 300 Hz; the plateau value is used. All fluids were verified as Newtonian. See ESI for details.

2.3 Droplet Size and Distribution Measurement

We analyze bright field optical micrographs for droplet size distribution using the Hough circle transform (ImageJ) on $\geq$ 300 droplets per sample. For samples with high hexane concentration ($\geq$ 55 wt_o%), low surface tension resulted in less spherical droplets, making the built-in plug-in unreliable. These droplets were measured manually. See ESI for details.

2.4 Emulsion Stability Limit Determination

Eight oil phases of varying hexane content are made for three SNP concentrations (Table 1, row 1). Starting with 3 g of the oil phase, we add the water phase in 2 g increments, first manually mixing, then DAC mixing (3500 rpm; 30 s). The emulsion is observed for 1 min for signs of aqueous phase coalescence. (A small amount of food coloring in the aqueous phase aids visual inspection.) If no coalescence occurs, the process is repeated. When coalescence occurs, excess water is removed and weighed to determine the emulsified quantity.

2.5 Synthesis of Closed-cell PolyHIPEs

Closed-cell polyHIPEs utilize the emulsion fabrication procedure in Section 2.1 for sample compositions in Table 2. Emulsions are transferred to 15 mL centrifuge tubes and centrifuged for 30 min (Fig.1) at the forces given in Table 2. After centrifugation, samples cure at 70 °C for 30 min then at room temperature for 24 h.

2.6 Synthesis of Open-cell PolyHIPEs

The method for making open-cell polyHIPEs resembles that used for closed-cell polyHIPEs (Sections 2.1 & 2.5). Sylgard 184 in a prepolymer:crosslinker ratio of 5:1 is the oil phase. The aqueous phase is blended into the oil phase in the presence of 10% surfactant (Gransurf 2106) at 1500 rpm and centrifuged at 2800g for 5 min. Centrifuged emulsions cure at 70 °C for 90 min.

2.7 Fractionation for Gradient Minimization

We use 2.8 wt_o% SNPs and 23 wt_e% aqueous phase. The aqueous phase is mixed into the continuous phase (600 rpm; 15 min) then subjected to a two-step centrifugation: 1) 1100g for 5 min then removal of the top 10 mL and bottom 1 mL of the centrifuged emulsion, 2) remaining emulsion poured into a partially glycerol-filled tube then centrifuged again (1300g, 1500g and 2000g, in that order; 3 min each).

2.8 PolyHIPE Microstructural Characterization

We analyze x-ray micro computed tomography (μCT) scans of the polyHIPEs (360° rotation; 4× magnification; 3 s exposure with binning value of 2; Source: 31.5 mm, Detector: 20 mm, Source Voltage: 66 kV, Source power: 8 W). Three dimensional reconstruction of the porous structure was not possible with the quality of images obtained due to the low density differential between the aqueous and polymerized phases. However, single slices may be analyzed. Slices corresponding to the same heights within a tube are analyzed. See ESI for details of image processing for determining area fraction and cavity size distribution.

We observe dried, uncoated polyHIPE cross-sections ($\approx$ 2 mm thick) in a Phenom Pro scanning electron microscope (*Nanoscience Instruments*; 5 kV; standard holder) to determine wall thickness distributions (See ESI). Cross-sections dry at room temperature for 24 h to remove water prior to imaging.

3 Results and Discussion

Control of the final porous microstructure relies on the ability to tune droplet size and size distribution within HIPE emulsions. Direct HIPE fabrication however is extremely limited at low viscosity ratios, $\lambda = \eta_a/\eta_c$ (aqueous phase viscosity, η_a; continuous phase viscosity, η_c). These limitations, combined with cure inhibition at larger viscosity ratio (higher hexane weight fraction), necessitate the use of centrifugation of LIPEs[22–24] as the starting point for polyHIPE fabrication.[‡]

LIPE templates comprised of the continuous/aqueous phases presented here produce mean droplet diameters of 20 - 100 μm. Upon centrifugation, LIPEs produce stable HIPEs we cure to form polyHIPEs (Fig. 1). Final polyHIPE microstructure thus varies with the LIPE droplet structure, droplet resistance to coalescence (achieved via surface active silica nanoparticles), and centrifugation force. Though centrifugation induces a microstructural gradient, we demonstrate gradient mitigation through a fractionation procedure. We focus here on the production of uniquely closed-cell, high-dispersed-phase-volume-fraction aqueous-in-silicone polyHIPE composites, but give an example of how related open cell structures might be obtained using surfactant for potential use as co-continuous composite frameworks.

3.1 Emulsion Template Control

Limitations on the stability of HIPEs from Pickering emulsions, which often invert at dispersed volume percents above 70%,[25]

[‡] LIPE's are defined as emulsions having internal phase volumes of < 30%.

Effect Studied	SNP (wt_o%)	Hexane (wt_o%)	Aqueous phase (wt_e%)	Speed (rpm)
Stability Limit	2, 3, 4	0 - 64	28 $\rightarrow$ saturation	3500
Viscosity Ratio	3	20 - 64	23	2000
Emulsion Stabilizer	2, 3, 4	50	23	3500
Mixing Speed	3	50	23	1500 - 3500

Table 1 Emulsion sample compositions and processing conditions. wt_o% or wt_e% indicate the percent by weight of the oil phase or the emulsion, respectively.

Effect Studied	SNP (wt_o%)	Hexane (wt_o%)	Aqueous phase (wt_e%)	Speed (rpm)	Centrifugal Force (g)
Emulsion Stabilizer	1.6 - 3.2	20	23	3500	3000
Centrifugal Force	3	20	23	3500	1800 - 3000

Table 2 Polymerized sample compositions and processing conditions.

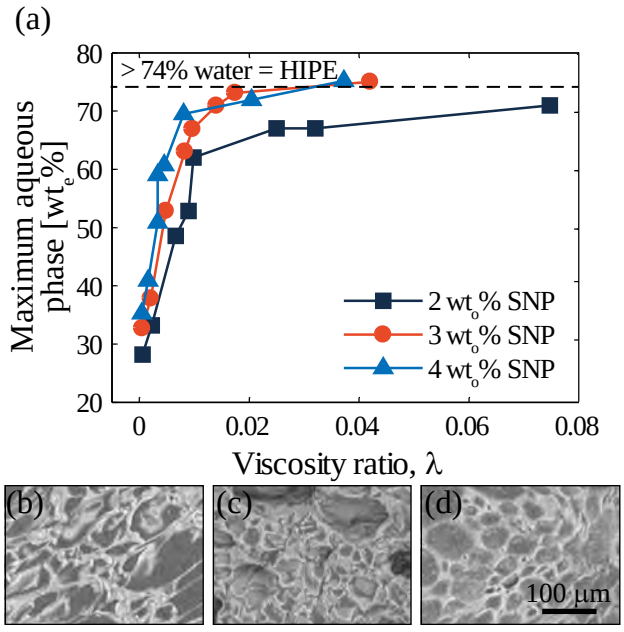

Fig. 2 Effect of viscosity ratio. (a) Maximum amount of aqueous phase that can be added to an emulsion by shear mixing as a function of increasing viscosity ratio with 2 (dark blue-squares), 3 (red-circles), and 4 (light blue-traingles) wt_o% SNP. (b-d) SEM micrographs of polymerized emulsions consisting of 64 wt_o% hexane and stabilized with (b) 2 wt_o%, (c) 3 wt_o%, and (d) 4 wt_o% SNP concentrations, each corresponding to the largest λ value samples plotted in (a).

and the difficulty of droplet breakup at low viscosity ratio requires droplet control considerations for LIPEs. The latter increases microstructural flexibility by enabling use of a wider range of fabrication parameters.

3.1.1 Water Content Limitations

Undiluted by hexane, less than 35 wt_e% of the aqueous phase (water+glycerol+NaCl) may be emulsified in the highly viscous oil phase (silicone pre-polymer + SNP) (4865 cP, 4 wt_o%) under the processing conditions described in Section 2.1. We attribute this limitation to two key parameters known to govern droplet break-up in Newtonian fluids:[17] the viscosity ratio between the components, $\lambda = \eta_d/\eta_c$, and the capillary number*, Ca, which accounts for the relative contributions from shear stress, leading to droplet deformation, and the Laplace pressure, preventing break-up (See ESI for further discussion of Ca limitations for droplet breakup as a function of λ, *i.e.*, modifications of the Grace curve[17]). We find that emulsions with higher viscosity ratios stabilize more water (Fig.2(a)),[26] but also that for the range of compositions tested (Tab. 1) a HIPE only forms for SNP compositions ≥ 3 wt_o% and only at the highest hexane concentrations prepared (64 wt_o%) (Fig. 2(a)). Interestingly, we observe these Pickering HIPEs even in the absence of careful tuning of the colloidal particle surface as has often been required.[4,22,23,27–29] This stability may be temporary, as coarsening or inversion could be slowed by the high viscosity continuous phase.

Lower viscosity ratio formulations demand higher capillary number corresponding to higher applied shear stress during mixing to achieve droplet breakup (See ESI for details). For this reason, most emulsions, especially HIPEs, made using shear mixing or microfluidics have a $\lambda \geq 0.01$.[16,30–32] Despite the ability to reach HIPE compositions at two SNP concentrations, the single mixing speed required (highest possible in our DAC mixer) provides no additional microstructural control. More importantly, evaporation of the large quantity of hexane present in the HIPE samples that do form (Fig. 2(b-c)), distorts the desired closed-cell, microstructure and inhibits curing. Creases and irregularities visible in the walls of the cells (Fig. 2(b-d)) are thought to be the result of evaporation of the significant hexane content during curing as we do not observe them in the structures produced with lower hexane content.

3.1.2 Droplet Tuning

Mean droplet size and size distribution vary with emulsion stabilizer concentration, mixing speed, and viscosity ratio. Emulsion stabilizer (SNP) concentration exhibits a saturation behavior we associate with achieving the minimum required interfacial cover-

* $Ca = \frac{\tau}{2\sigma/d}$ with τ, σ, and d being the shear stress, surface energy, and droplet diameter, respectively.

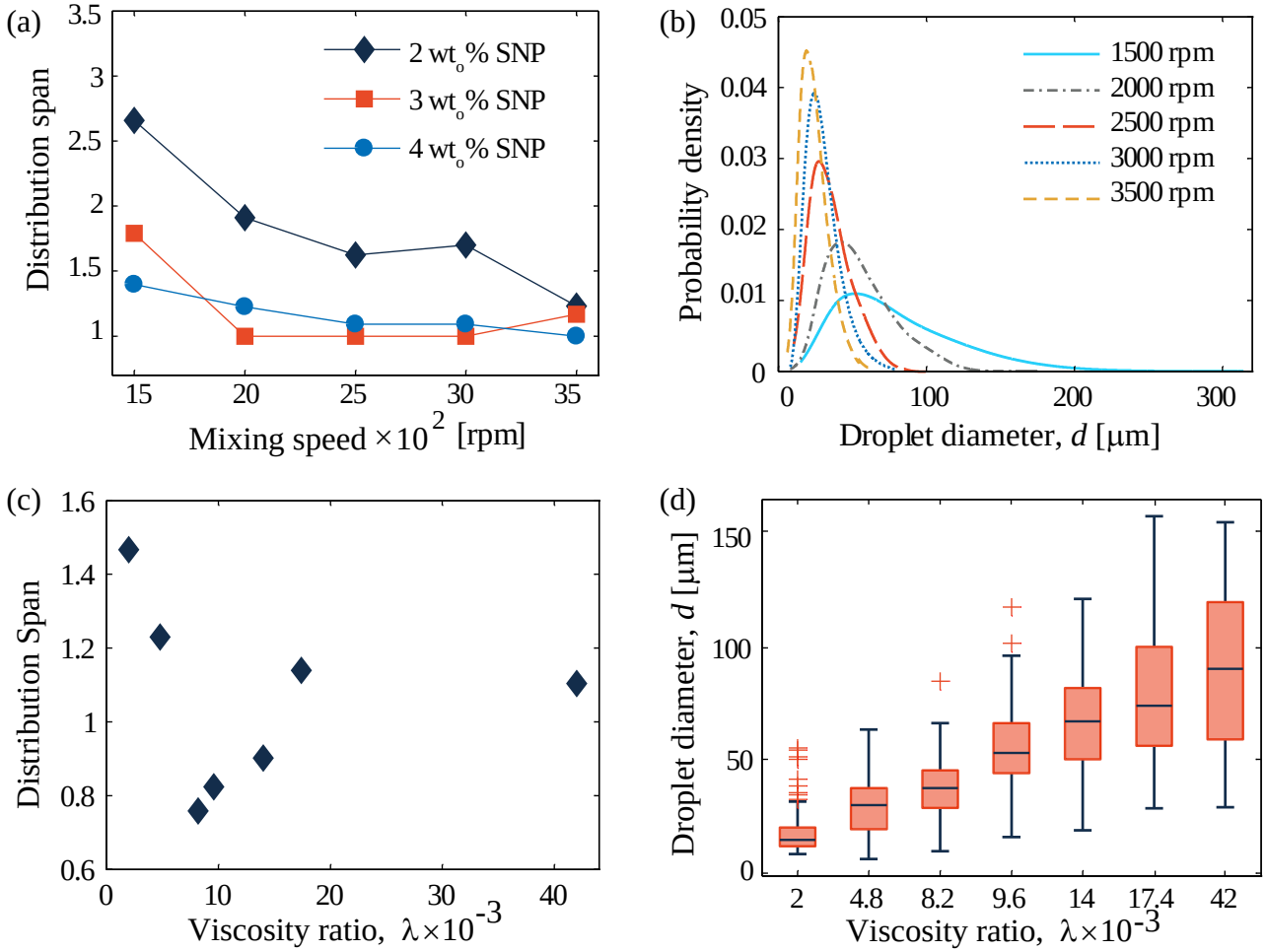

Fig. 3 Effect of emulsion stabilizer, mixing speed, and viscosity ratio on emulsion droplets. (a) Distribution span of emulsions with 2 (dark blue-diamonds), 3 (red-squares), and 4 (light blue-circles) wt$_o$% SNP concentrations mixed at different speeds. (Emulsions: 23 wt$_e$% aqueous phase, 50 wt$_o$% hexane, λ = 0.01, 0.009 and, 0.004 for 2, 3 and, 4 wt$_o$% SNP, respectively).(b) Probability densities for emulsions mixed at 1500, 2000, 2500, 3000, and 3500 rpm with 3 wt$_o$% SNP concentration. All distributions are lognormal. (c) Distribution span of the emulsion droplets as a function of increasing viscosity ratio. (Emulsions: 3500 rpm, 23 wt$_e$% aqueous phase, 3 wt$_o$% SNP). (d) Droplet size as a function of viscosity ratio. Boxes correspond to the 25th and 75th percentiles. The inner horizontal line indicates the median and the ends of whiskers show the extreme values of the data set by disregarding the outliers. Outliers (values >1.5 times the interquartile range from top and bottom of the box) are indicated with plus signs.

age for droplet stability, while mixing speed provided the greatest practical means of tuning mean droplet size. However, changes in mean droplet size were associated with variation in size dispersity.

We observe a saturation behavior associated with increasing emulsion stabilizer concentration. Droplet size distributions approach a similar form for 3 and 4 wt$_o$% (Fig. S6). Droplet uniformity decreases for the lowest SNP concentration, 2 wt$_o$%, suggesting insufficient surface coverage. Uniformity is quantified in Fig. 3(a) using the span of the distribution, S, determined via

$$S = \frac{D_{90} - D_{10}}{D_{50}}. \quad (1)$$

Here D_{90}, D_{10}, and D_{50} are the 90th, 10th, and 50th percentile of the data. For the range of mixing speeds tested, significant differences in the droplet size distributions were observed for all 2 wt$_o$% SNP concentrations relative to either the 3 or 4 wt$_o$% formulations. At most speeds, 4 wt$_o$% formulations had less or equal size uniformity relative to the 3 wt$_o$% (only for 2000 rpm was S higher, $p = 0.47$). These minimal changes in the size distributions at high SNP concentration and decreased uniformity at low concentration are consistent with the interpretation that 3 wt$_o$% is near the onset of total surface coverage for droplets formed within the 23 wt$_e$% aqueous emulsions characterized over this range of mixing speeds.

Of the parameters tested, mixing speed had the largest and most readily controlled effect on $\bar{d}$. Droplet diameter and non-uniformity both increase with decreasing mixing speed (Figure 3(b)). Mean droplet diameters indicate an $\sim 3.5\times$ increase in $\bar{d}$ (25 - 87 μm) accompanying a 3/7 reduction in mixing speed. Over this same range of speeds, S increases by only $\sim 1.5\times$. Droplet distribution control via changing viscosity ratio (through the addition of hexane in the continuous phase) is both less sensitive and less systematic. In Fig. 3(d), box-whisker plots indicate that over a 21$\times$ increase in λ, from 0.002 to 0.042 (3-fold increase in hexane content), we observe a 5.3$\times$ increase in $\bar{d}$ (17

to 90 μm). For this same viscosity range, the span first decreases to a minimum value of 0.75 at $\lambda = 0.008$ and then gradually increases to reach a plateau of S $\sim$ 1.1 at viscosity ratios above 0.017 (Fig. 3(c)). We do not have an explanation for this behavior. The other drawback to utilization of the full viscosity range is that for hexane content above 60 wt$_o$% ($\lambda = 0.017$), we observe only surface layer curing of the polyHIPE after 5 days of observation.

The observations discussed above enable tuning of the final closed-cell pore size. For example, we can achieve a lower droplet size limit of $\bar{d} = 6.95$ μm with S = 0.88 (20 wt$_o$% hexane, $\lambda = 1.6 \times 10^{-3}$, 3500 rpm, and 23 wt$_e$% aqueous phase). Several other composition/parameter combinations were performed to validate the trends reported in Fig. 3 and can be found in the ESI (Fig. S7).

3.2 Closed-cell polyHIPEs

We demonstrate droplet concentration via centrifugation. SNPs stabilize against droplet coalescence. We validate this stabilizing and weakly size-modifying effect of SNPs via a study of the final, cured structure. For a range of processing conditions we observe mechanically robust, closed-cell polyHIPEs (Figure 4) with aqueous content reaching 82 % by volume (see ESI for flame resistance, similar to Gurevitch and Silverstein [5], and squeeze test demonstrations).

3.2.1 Microstructural Features

Upon curing of the PDMS phase, HIPEs result in an elastomeric composite having liquid inclusions. The microstructure of these monoliths is observed using μCT scanning of as-fabricated samples and SEM imaging of lateral cross sections. The representative image shown in Fig. 4 illustrates the closed-cell elastomeric structure (aqueous-phase removed). The non-spherical cells are indicative of the droplet deformation characteristic of HIPEs. The smooth wall surface demonstrated in Fig. 4 is found, by trial-and-error, to occur with high temperature initial curing (Section 2.5) that presumably causes quick evaporation of the hexane prior to network formation.

3.2.2 Dependence on Centrifugation

Centrifugation of LIPEs can create HIPEs, but only in the absence of droplet coalescence. Owing to differences in density between the continuous (oil+SNP) phase and dispersed (aqueous) phase, the aqueous droplets condense at high centrifugal load. As a result, centrifugation is often used as a means to verify the stability of an emulsion. [33–37] As a high gravity extension of the creaming typically observed in emulsions, centrifugation also concentrates droplets within an emulsion. [38–40] It follows that the strength of the centrifugal force determines the degree of packing between stabilized droplets. [38] However, to our knowledge no systematic study of this effect on the resulting microstructure has been quantified for polyHIPEs.

For consistency, we select a constant centrifugation time that ensures all macroscopic droplets settle. We estimate the settlement time, t_s, for the aqueous phase droplets using Stokes' Law, [41,42]

$$t_s = \frac{4\eta_c h}{(\rho_d - \rho_c) d^2 N \mathrm{g}}, \qquad (2)$$

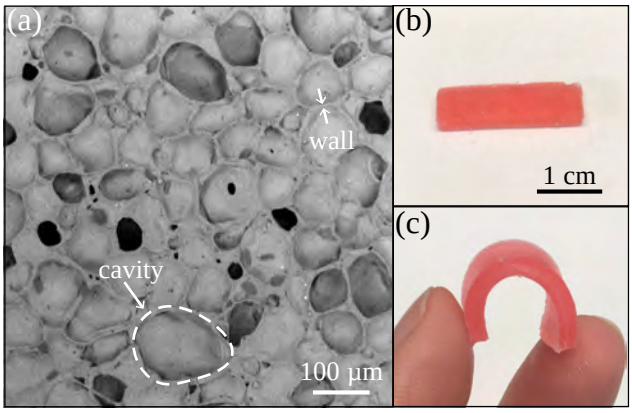

Fig. 4 Closed-cell, aqueous-filled, silicone polyHIPEs. (a) SEM micrograph of a Pickering polyHIPE made with aqueous droplets in PDMS (water removed by drying the c/s). The cavity walls are closed with no pore throats or defects. Note that the cavities are highly polyhedral. (b) Digital image of a Pickering polyHIPE cured in a rectangular mold. (c) The polyHIPE bends, without any structural disintegration, upon application of manual force. (3000g. Emulsion templates: 23 wt$_e$% aqueous phase, 20 wt$_o$% hexane, 3 wt$_o$% SNP)

where η_c is the viscosity of the continuous phase, h is the settlement distance to be travelled by the droplet, ρ_d and ρ_c are the dispersed and continuous phase densities, respectively, d is the droplet diameter, N is a gravitational multiplication factor and $\mathrm{g} = 9.81$ m/s^2 is the acceleration due to gravity (*i.e.*, for a centrifugal force of 2000g, $N = 2000$). We estimate an upper limit of $t_s = 20$ min assuming the most viscous continuous phase ($\eta_c = 1.07$ Pa.s, $\rho_c = 849.37$ kg/m^3) used and a small drop ($d = 20$ μm, $\rho_d = 1064.7$ kg/m^3) situated at the top of the centrifuge tube ($h = 8$ cm) under the smallest centrifugal force we consider ($N\mathrm{g} = 1800\mathrm{g}$). With the majority of the droplets in our emulsions in the range of 20-150 μm, a centrifugation time of 30 min assures that all of the droplets will form a concentrated emulsion.

Stronger centrifugal forces increase the aqueous volume fraction. This effect is moderate over experimentally accessible ranges. Samples fabricated from 3 wt$_o$% SNP emulsions centrifuged at forces ranging from 1800g to 3000g (Fig. 5) demonstrate only a 10% relative increase in volume fraction (Fig. 6(a)). However, average wall thickness decreases from 13 to 1.5 μm, nearly an order of magnitude, over this same range of centrifugation forces (Fig. 6(b)). Simultaneously, wall thickness uniformity increases. Droplets templated by the original emulsion remain intact for all but the highest forces used. As Figures 6(c) & (d) illustrate, cavity size and distribution remain unchanged for forces up to 2700g. Only at the highest centrifugal force tested (3000g), does the mean cavity size increase. A potential reason for this increase is that higher centrifugal forces deform, rupture, and eventually merge some of the original droplets into larger droplets. In support of this mechanism, we compare the cavity size distributions of the centrifuged samples to the droplet distribution of the low internal phase emulsion (LIPE) used to make the HIPEs. A Mann-Whitney U-test between the LIPE (black, long-dash double-dot curve) and each preparation condition confirms

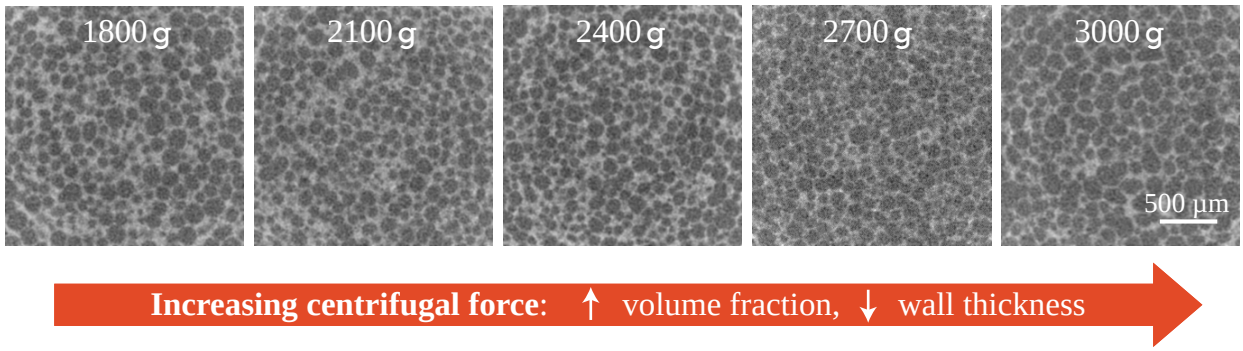

Fig. 5 MicroCT cross-sections of polyHIPEs formed under varying centrifugal forces. Lighter regions indicate the polymerized oil phase while the dark grey areas denote the higher density aqueous phase. (Emulsion templates: 23 wt_e% aqueous phase, 20 wt_o% hexane, 3 wt_o% SNP)

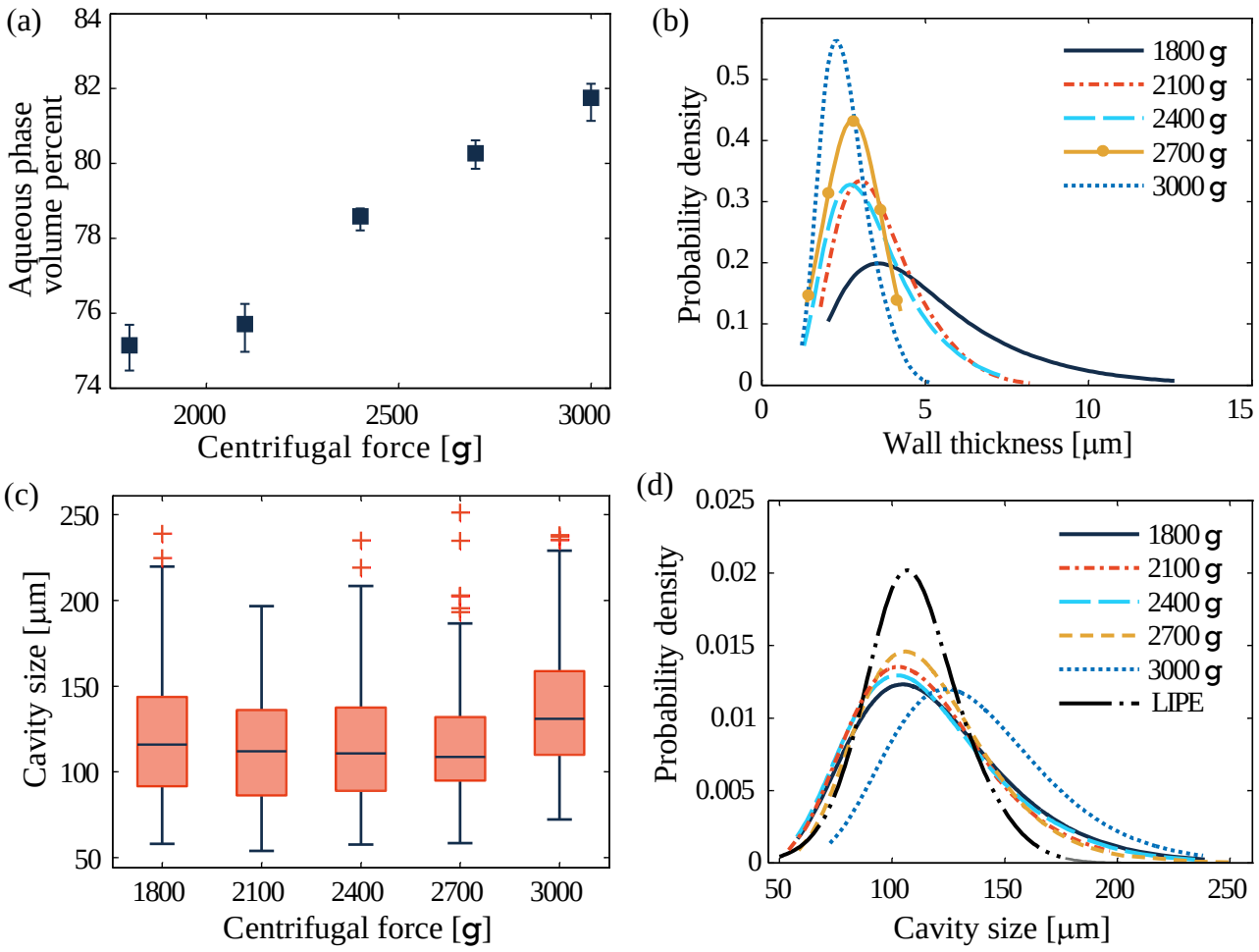

Fig. 6 Effect of centrifugal force on polyHIPE microstructure. (a) Aqueous phase volume fraction as a function of increasing centrifugal force. Error bars correspond to the standard deviation from 5 images. (b) Wall thickness probability densities for centrifugal forces of 1800g (dark blue-solid), 2100g (red-dash dotted), 2400g (teal-dash), 2700g (yellow-solid with circles), and 3000g (light blue-dotted). All distributions are best described as lognormal except 2700g (normal). (c) Droplet diameter at 1.2 mm from the bottom of the polyHIPEs as a function of increasing centrifugal force. Only the 3000g sample is statistically significantly different. Boxes correspond to the 25^{th} and 75^{th} percentiles. The inner horizontal line indicates the median and the ends of whiskers show the extreme values of the data set by disregarding the outliers. Outliers (values >1.5 times the interquartile range from top and bottom of the box) are indicated with plus signs. (d) Cavity size probability densities considering cross-sections ranging from bottom of the samples to a height of 4 mm compared for centrifugal forces ranging from 1800 to 3000g. The black (long-dash double-dot) curve corresponds to the droplet diameter distribution of the LIPE template emulsion used. Except for the sample centrifuged at 3000g, the probability density curves are same (including the LIPE distribution) within a 95% confidence level. All the distributions are lognormal. (Emulsion template: 23 wt_e% aqueous phase, 20 wt_o% hexane, 3 wt_o% SNP)

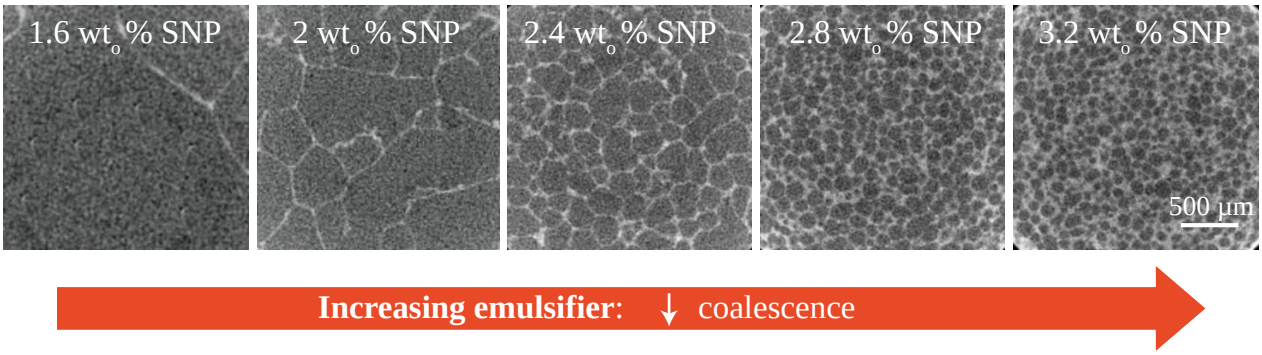

Fig. 7 MicroCT cross-sections of polyHIPEs formed at varying SNP concentration. Lighter regions indicate the polymerized oil phase while the dark grey areas denote the higher density aqueous phase. (3000g. Emulsion templates: 23 wt$_e$% aqueous phase, 20 wt$_o$% hexane)

that the cavity size distribution of the 3000g sample is the only sample that is statistically significantly different from that of the templating emulsion ($p = 1.3 \times 10^{-5}$).

3.2.3 Dependence on SNP Concentration

We determine the minimum SNP concentration for stable HIPEs capable of sustaining the high centrifugal forces required for high volume fraction. Fig. 7 illustrates the polyHIPE microstructures prepared at different SNP concentrations (in the emulsion) for the highest centrifugal force (3000g). (Note that SNP content changes upon curing due to evaporation of hexane.) It is clear from these images that significant coalescence occurs for SNP concentrations at and below 2 wt$_o$%. These small quantities of nano-particles appear to be insufficient to cover the droplet interface. We therefore analyze volume fraction, wall thickness, and cavity size for the higher concentration samples. As Figure. 8(a) shows, volume fraction decreases with increasing SNP content. This trend can be understood through the decrease in droplet diameter across the entire range of SNP parameters ($p < 10^{-5}$ for all distributions) (Fig. 8(c) & (d)), *i.e.*, more walls are present in the sample. Notably, wall thickness appears to approach a plateau, perhaps due to steric interaction between the particles, with no statistically-significant difference found between the 2.8 and 3.2 wt$_o$% formulations ($p = 0.51$) (Fig. 8(b)).

3.2.4 Structural Gradient and Gradient Minimization via Fractionation

Under traditional, one-step centrifugation, non-uniform samples settle sequentially as a function of size due to differences in drag/forcing. The result is a gradient in the cavity size in the final, cured polyHIPE, with cavity size reducing, as expected, with increasing distance from the bottom, D (Fig. 9(a)). While this gradient may be desirable for some applications, often it is useful to minimize it. We find that for all centrifugation forces, ranging from 1800 to 3000g, a statistically significant gradient in average cavity diameter exists, but the difference between these gradients is not statistically significant, consistent with results reported in Sec. 3.2.2. The gradient is a direct consequence of the droplet settlement time being inversely proportional to the square of the droplet radius (Eqn. 2). Because cavities closer to bottom of the sample are associated with droplets with shorter settlement time ($D \sim t$), Eqn. 2 predicts $d \sim D^{-1/2}$. We do not observe this exact scaling due to the interaction between droplet distribution and the conically-shaped tip of the centrifuge tube within which the gradient is measured, however, the trend lies in the same direction. The average percent difference between 0.2 and 3.8 mm from the sample bottom is 43%.

To eliminate the observed gradient, we perform a fractionation procedure, which is a two-step centrifugation process (described in detail in Section 2.7). We find no significant gradient in cavity size across the range of D observed as indicated by a flat profile (Fig. 9(b)), as opposed to the graded one in Fig. 9(a). Fig. 9(c) demonstrates that the probability density curves for cavity size at progressively larger D are also unchanged. The consistent, overlapping curves with $p \geq 0.05$ for all cases, correspond to a mean droplet diameter of about 100 μm at each interval (1.2 cm thick cylindrical sample).† Analysis of the volume fraction as a function of D (Fig. 9(d)) also finds no gradient and validates that the composite lies within the high internal phase regime (79% - 82% water by volume). Thus, the fractionation method eliminates gradients within the polyHIPEs.

3.3 Open Cell polyHIPEs

In contrast to SNPs, using a molecular surfactant imparts an open-cell structure to the polyHIPE as previously observed.[43] Sylgard 184 and surfactant (Gransurf 2106) with no hexane was used to produce the structure in Figure 10. The resulting cavities are spherical with interconnects, known as pore throats, allowing free flow of the aqueous phase out of the polymer structure. Surfactant molecules maintain an equilibrium concentration at the surface, thereby preferring the spherical droplet geometry that leads to open-cell HIPE structures. In contrast, droplets covered with SNPs act like elastic shells and allow for nano-particle redistribution, rather than desorption, accompanying changes in interfacial area.[44] This elasticity allows droplets, upon being subjected to compressive forces, to deform into polyhedrons and results in dense packing densities that form a closed-cell HIPE.

† $S = 0.88$ within the observed region.

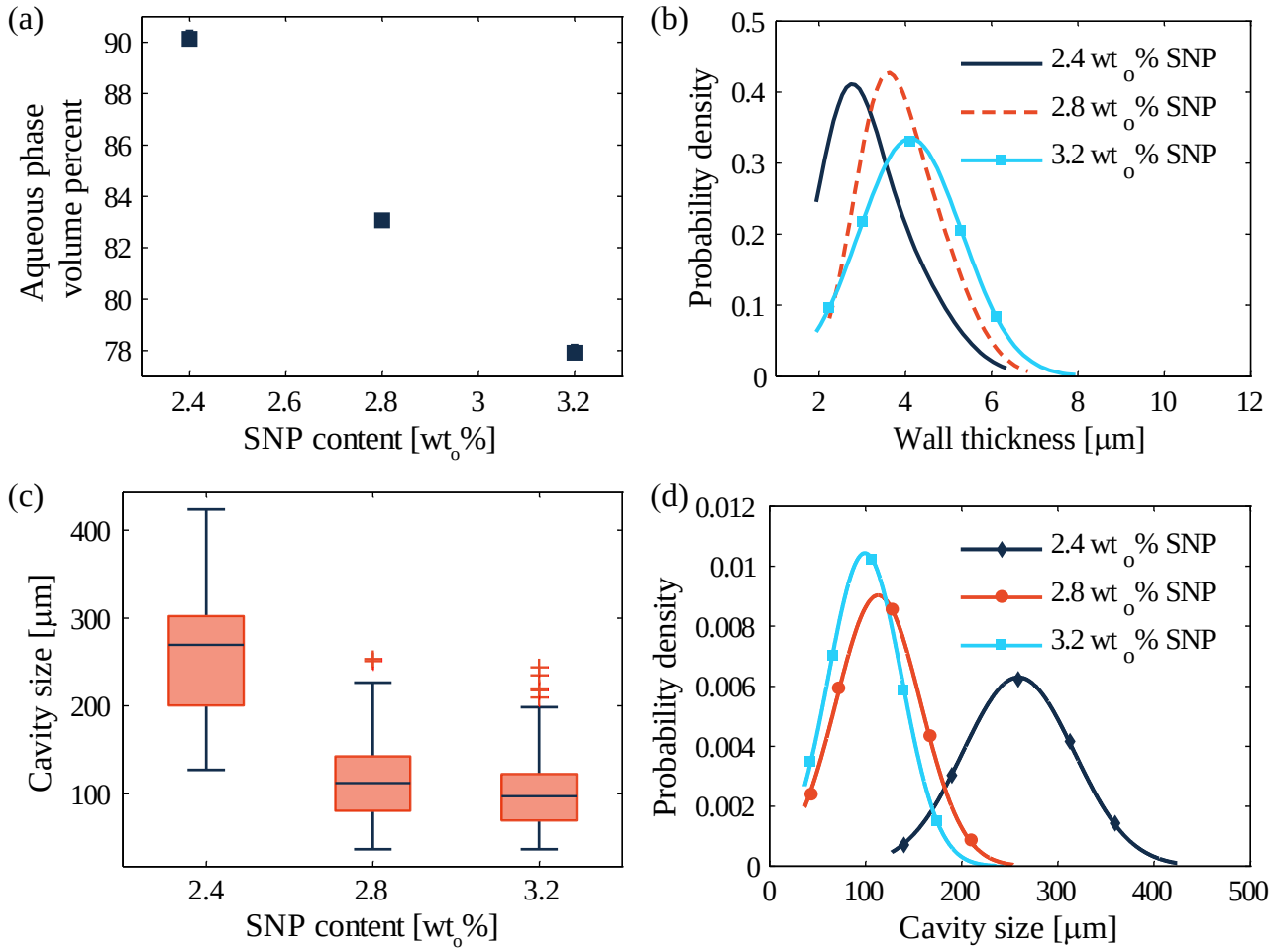

Fig. 8 Effect of SNP concentration on polyHIPE microstructure. (a) Aqueous phase volume fraction as a function of increasing SNP concentration. (b) Probability densities for wall thicknesses of 2.4 (dark blue-solid), 2.8 (red-dash), and 3.2 (teal-solid with squares) wt_o% SNP compositions follow lognormal, lognormal, and normal distribution functions, respectively. (c) Cavity size as a function of SNP concentration. Boxes correspond to the 25^{th} and 75^{th} percentiles. The inner horizontal line indicates the median and the ends of whiskers show the extreme values of the data set by disregarding the outliers. Outliers (values >1.5 times the interquartile range from top and bottom of the box) are indicated with plus signs. (d) Probability densities for cavity size of 2.4 (dark blue-solid with diamonds), 2.8 (red-solid with circles), and 3.2 (teal-solid with squares) wt_o% SNP compositions. All distributions are normal. (3000g. Emulsion template: 23 wt_e% aqueous phase, 20 wt_o% hexane)

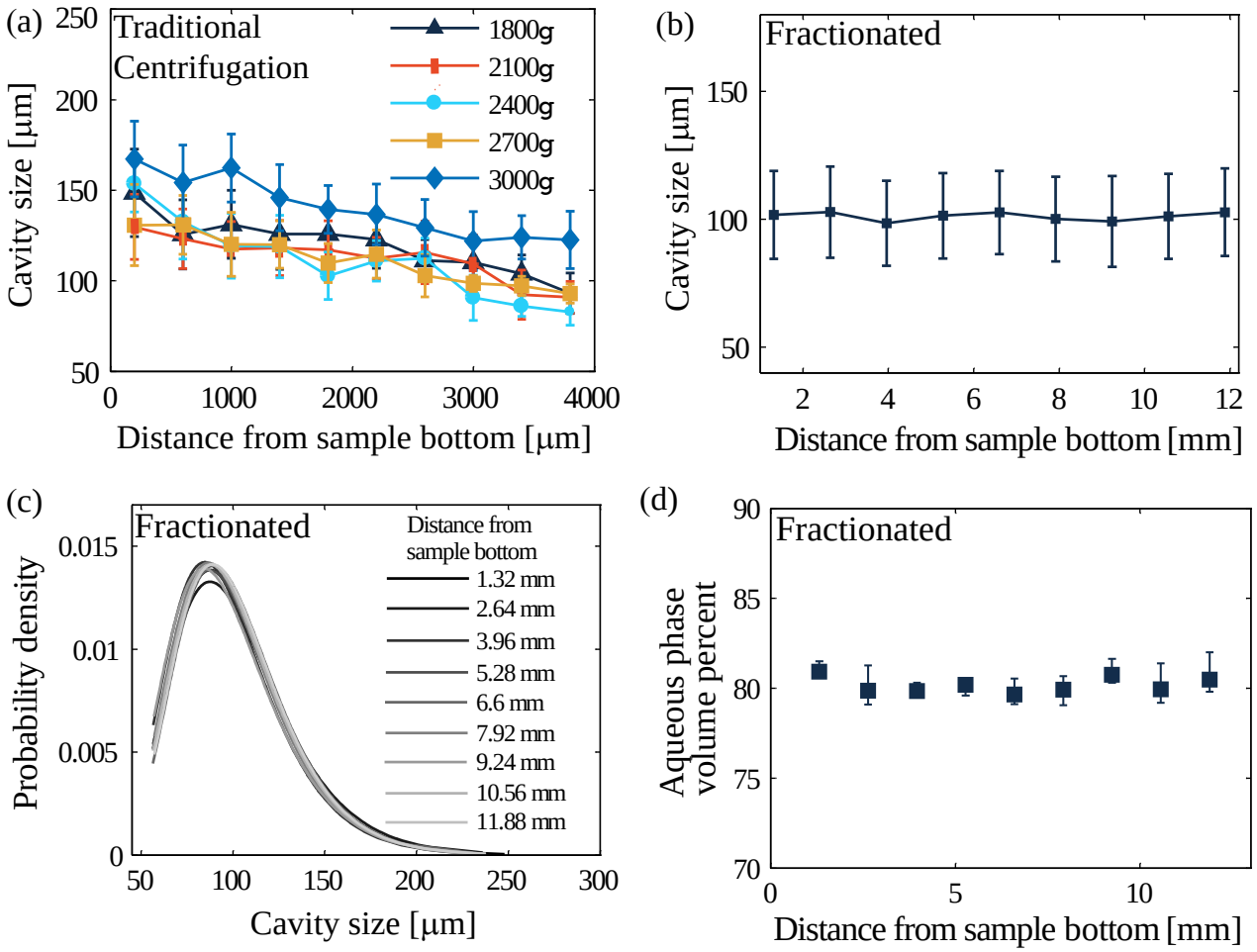

Fig. 9 PolyHIPE composite structure. (a) Average cavity size as a function of the distance from the bottom of the sample, D, for centrifuged, closed-cell polyHIPEs. For all centrifugation forces, cavity size reduces as we move away from the bottom of the sample. Error bars indicate standard deviation at each of the locations. (b) A flat cavity size profile associated with the structure obtained with the additional fractionation step. (c) Overlapping probability distributions for cavity size at increasing D (black = bottom, lightest gray = top). All distributions are lognormal (mean size = 100 μm). (d) Aqueous phase volume fraction as a funciton of D for a polyHIPE made by the fractionation method. Error bars show the variation in 5 consecutive images. (3000g. Emulsion template: 23 wt_e% aqueous phase, 2.8 wt_o% SNP, 20 wt_o% hexane)

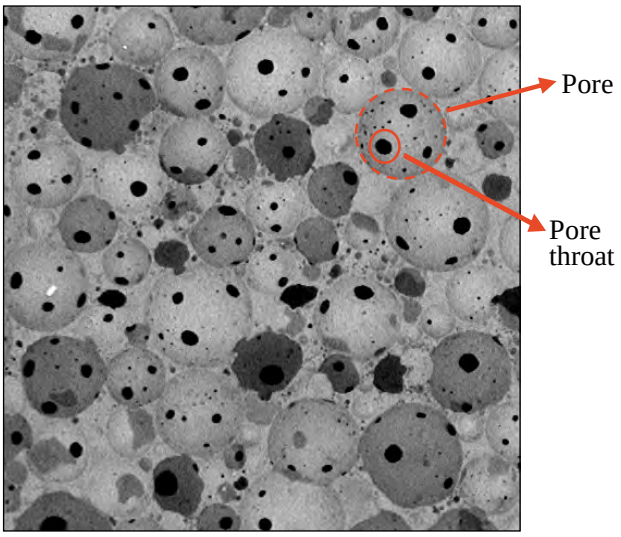

Fig. 10 SEM micrograph of an open-cell polyHIPE made using molecular surfactant. Note the highly spherical pores connected via circular pore throats where pores come into contact.(2800g. Emulsion template: 23 wt_e% aqueous phase, 10 wt_o% Gransurf 2106, Sylgard 184 in 5:1 ratio)

4 Conclusions

This work provides, for the first time, fabrication methods and microstructural control mechanisms for the creation of closed-cell, aqueous-filled silicone polyHIPE composites using commercially-available materials and processes. Utilizing centrifugation to overcome limitations on the aqueous phase volume fraction when using a high viscosity continuous phase (low viscosity ratio), we produce both open and closed-cell structures. We also provide a method for elimination of the centrifugation-induced microstructural gradient. Monolithic, macroscopic, mechanically robust polyHIPE composites with cavities of biologically-relevant sizes (20 to 100 μm) are now possible using this combination of approaches, *i.e.*, colloidal stabilization of droplets and centrifugal concentration of LIPEs, where application of each separately would be ineffective.

To facilitate the future application of these novel materials, we report droplet size distributions and variations for water-in-oil (aqueous-in-PDMS) LIPEs as a function of processing parameters (mixing speed) and composition (continuous phase viscosity and SNP-emulsifier concentration). The observed distributions are consistent with those observed in the polyHIPE structures, which effectively 'freeze' the emulsion templates into the final closed-cell structure. Both decreased mixing speed and continuous phase viscosity produce larger template droplets. SNPs at sufficiently high concentration (~ 3 wt_o%) effectively stabilize the droplets at all but the highest centrifugation speeds.

We expect aqueous phase stability limits, droplet size distributions, and critical SNP concentrations to vary somewhat with changes in the aqueous phase (*i.e.*, the absence of glycerol, more or less salt, or the addition of biomedically-relevant solutes). However, preliminary tests suggest that the overall trends reported here will still guide future efforts to control PDMS-based, fluid-solid composite microstructure. The approach outlined here (Pickering emulsions concentrated via centrifugation) may also prove useful for other commercially-available, high viscosity polymers desired for liquid composite elastomers fabrication.

Conflicts of interest

There are no conflicts to declare.

Acknowledgements

This material is based upon work supported by the National Science Foundation under Grant No.(1653676). The authors also thank Prof. Randy Ewoldt and Yilin Wang for helpful discussion and viscosity measurements.

Notes and references

1 M. S. Silverstein, *Prog. Polym. Sci.*, 2014, **39**, 199–234.
2 M. S. Silverstein, *Polymer*, 2017, **126**, 261–282.
3 Y. Yang, Z. Fang, X. Chen, W. Zhang, Y. Xie, Y. Chen, Z. Liu and W. Yuan, *Front. Pharmacol.*, 2017, **8**, 287.
4 I. Gurevitch and M. S. Silverstein, *J. Polym. Sci., Part A: Polym. Chem.*, 2010, **48**, 1516–1525.
5 I. Gurevitch and M. S. Silverstein, *Macromolecules*, 2012, **45**, 6450–6456.
6 C. W. Damouny and M. S. Silverstein, *Polymer*, 2016, **82**, 262–273.
7 D. Zhu, S. Handschuh-Wang and X. Zhou, *J. Mater. Chem. A*, 2017, **5**, 16467–16497.
8 T. Kobayashi, H. Saitoh, N. Fujii, Y. Hoshino and M. Takanashi, *J. Appl. Polym. Sci.*, 1993, **50**, 971–979.
9 J. J. Chruściel and E. Leśniak, *J. Appl. Polym. Sci.*, 2011, **119**, 1696–1703.
10 A. Turco, E. Primiceri, M. Frigione, G. Maruccio and C. Malitesta, *J. Mater. Chem. A*, 2017, **5**, 23785–23793.
11 M. Tebboth, Q. Jiang, A. Kogelbauer and A. Bismarck, *ACS Appl. Mater. Interfaces*, 2015, **7**, 19243–19250.
12 J. Wang, M. Yu and C. Yang, *Colloids Surf., A.*, 2019, **570**, 224–232.
13 S. Jung, J. H. Kim, J. Kim, S. Choi, J. Lee, I. Park, T. Hyeon and D.-H. Kim, *Adv. Mater.*, 2014, **26**, 4825–4830.
14 R. Tutika, S. Kmiec, A. T. Haque, S. W. Martin and M. D. Bartlett, *ACS Appl. Mater. Interfaces*, 2019, **11**, 17873–17883.
15 A. Giustiniani, P. Guégan, M. Marchand, C. Poulard and W. Drenckhan, *Macromol. Rapid Commun.*, 2016, **37**, 1527–1532.
16 J. Schröder, A. Kleinhans, Y. Serfert, S. Drusch, H. P. Schuchmann and V. Gaukel, *J. Food Eng.*, 2012, **111**, 265–271.
17 H. P. Grace, *Chem. Eng. Commun.*, 1982, **14**, 225–277.
18 B. Bentley and L. G. Leal, *J. Fluid Mech.*, 1986, **167**, 241–283.
19 R. A. Debruijn, *PhD thesis*, 1991.
20 K. Jansen, W. Agterof and J. Mellema, *J. Rheol.*, 2001, **45**, 227–236.
21 S. Niv, *MSc thesis*, Israel Institute of Technology, 2016.
22 A. Menner, V. Ikem, M. Salgueiro, M. S. Shaffer and A. Bismarck, *Chem. Commun.*, 2007, 4274–4276.

23 P. J. Colver and S. A. Bon, *Chem. Mater.*, 2007, **19**, 1537–1539.

24 I. Capron and B. Cathala, *Biomacromolecules*, 2013, **14**, 291–296.

25 K. Kim, S. Kim, J. Ryu, J. Jeon, S. G. Jang, H. Kim, D.-G. Gweon, W. B. Im, Y. Han, H. Kim *et al.*, *Nat. Comm.*, 2017, **8**, 14305.

26 M.-T. Grosse, M. Lamotte, M. Birot and H. Deleuze, *J. Polym. Sci., Part A: Polym. Chem.*, 2008, **46**, 21–32.

27 V. O. Ikem, A. Menner and A. Bismarck, *Angewandte Chemie International Edition*, 2008, **47**, 8277–8279.

28 Z. Zheng, X. Zheng, H. Wang and Q. Du, *ACS applied materials & interfaces*, 2013, **5**, 7974–7982.

29 D. Cai, J. H. Thijssen and P. S. Clegg, *ACS applied materials & interfaces*, 2014, **6**, 9214–9219.

30 S. Sugiura, M. Nakajima, N. Kumazawa, S. Iwamoto and M. Seki, *J. Phys. Chem. B*, 2002, **106**, 9405–9409.

31 K. van Dijke, I. Kobayashi, K. Schroën, K. Uemura, M. Nakajima and R. Boom, *Microfluid. Nanofluid.*, 2010, **9**, 77–85.

32 C. Dicharry, B. Mendiboure and J. Lachaise, 10th European Conference on Mixing, 2000, pp. 501–508.

33 R. D. Vold and R. C. Groot, *The Journal of Physical Chemistry*, 1962, **66**, 1969–1975.

34 B. Haney, D. Chen, L.-H. Cai, D. Weitz and S. Ramakrishnan, *Langmuir*, 2019, **35**, 4693–4701.

35 X. Li, J. Li, J. Gong, Y. Kuang, L. Mo and T. Song, *Carbohydr. Polym.*, 2018, **183**, 303–310.

36 X. Song, M. Lin, C. Song, Z. Shi and H. Zhang, *J. Biores. Bioprod.*, 2018, **3**, 134–138.

37 L. Dai, S. Yang, Y. Wei, C. Sun, D. J. McClements, L. Mao and Y. Gao, *Food. Chem.*, 2019, **275**, 246–254.

38 T. Krebs, D. Ershov, C. Schroen and R. Boom, *Soft Matter*, 2013, **9**, 4026–4035.

39 *Adv. Colloid Interface Sci.*, 2004, **108**, 49–61.

40 Y. Li, X. Liu, Z. Zhang, S. Zhao, G. Tian, J. Zheng, D. Wang, S. Shi and T. P. Russell, *Angew. Chem.*, 2018, **130**, 13748–13752.

41 C. J. Lentfer, M. M. Cotter and W. E. Boyd, *J. Archaeolog. Sci.*, 2003, **30**, 149–168.

42 D. C. Giancoli, *General physics*, Prentice Hall International, London, 1984.

43 V. O. Ikem, A. Menner, T. S. Horozov and A. Bismarck, *Advanced Materials*, 2010, **22**, 3588–3592.

44 L. Bécu and L. Benyahia, *Langmuir*, 2009, **25**, 6678–6682.

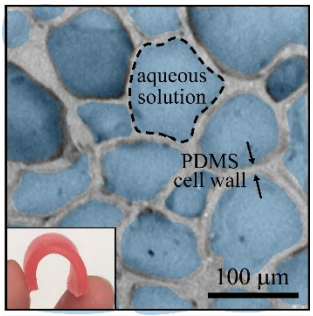

Elastomeric polyHIPE with aqueous encapsulations